Mn–Mg disordering in cummingtonite: A high-temperature neutron powder diffraction study

Article *in* Mineralogical Magazine · April 2000

DOI: 10.1180/002646100549166 · Source: OAI

4 authors, including:

Simon Redfern
Nanyang Technological University
398 PUBLICATIONS **8,942** CITATIONS

SEE PROFILE

Mark David Welch
Natural History Museum, London
142 PUBLICATIONS **2,118** CITATIONS

SEE PROFILE

Mineralogical Magazine, April 2000, Vol. 64(2), pp. 255–266

Mn-Mg disordering in cummingtonite: a high-temperature neutron powder diffraction study

J. J. Reece[1]*, S. A. T. Redfern[1], M. D. Welch[2] and C. M. B. Henderson[3]

[1] Department of Earth Sciences, University of Cambridge, Downing Street, Cambridge, CB2 3EQ
[2] Department of Mineralogy, The Natural History Museum, Cromwell Road, London, SW7 5BD
[3] Department of Earth Science, University of Manchester, Oxford Road, Manchester, M13 9PL, UK

ABSTRACT

The crystal structure of a manganoan cummingtonite, composition $^{[M4]}(Na_{0.13}Ca_{0.41}Mg_{0.46}Mn_{1.00})$ $^{[M1,2,3]}(Mg_{4.87}Mn_{0.13})[Si_8O_{22}](OH)_2$, ($Z = 2$), $a = 9.5539(2)$ Å, $b = 18.0293(3)$ Å, $c = 5.2999(1)$ Å, $\beta = 102.614(2)^\circ$ from Talcville, New York, has been refined at high temperature using *in situ* neutron powder diffraction. The $P2_1/m$ to $C2/m$ phase transition, observed as spontaneous strains $+\varepsilon_1 = -\varepsilon_2$, occurs at ~107°C. Long-range disordering between Mg^{2+} and Mn^{2+} on the M(4) and M(2) sites occurs above 550°C. Mn^{2+} occupies the M(4) and M(2) sites preferring M(4) with a site-preference energy of 24.6 ± 1.5 kJ mol^{-1}. Disordering induces an increase in X_{Mn}^{M2} and decrease in X_{Mn}^{M4} at elevated temperatures. Upon cooling, the ordered states of cation occupancy are 'frozen in' and strains in lattice parameters are maintained, suggesting that re-equilibration during cooling has not taken place.

Keywords: cummingtonite, order-disorder, cation partitioning, neuytron diffraction, phase transition.

Introduction

A quantitative knowledge of the temperatures and pressures of formation of mineral assemblages is fundamental to understanding the thermal evolution of the Earth, and to the development of well-constrained petrological and geophysical models. For some time, geothermometric and geobarometric deductions have been based on the compositional variations of coexisting rock-forming minerals (e.g. cation partitioning between orthopyroxene/clinopyroxene; orthopyroxene/garnet; magnetite/ilmenite). Information on cooling rates (geospeedometry) is also potentially available from the knowledge of intracrystalline cation site partitioning (e.g. cation ordering within pyroxene or olivine).

Amphiboles provide ideal candidates for application as thermometric indicators, since non-convergent cation ordering occurs within them as a function of temperature, and they are stable across a wide range of temperatures, pressures and rock compositions, corresponding to environments from the crust to the upper mantle (including important subduction environments). Very limited use has been made of amphiboles as thermometric indicators, however, because of their compositional and structural complexity, and a limited understanding of their thermodynamic properties. The crystal-chemical complexity that makes amphiboles such a challenge is itself a potential recorder of the thermal history of the mineral, and in so doing can lock away a wealth of information on the time-temperature paths of the rocks in which they are found. If a working knowledge can be established of the temperature dependence of cation ordering in amphiboles, a treasure-trove of thermometric petrological information is likely to become available.

This is the first part of a wider investigation into the temperature-dependent cation ordering within the cummingtonite-grunerite series, a group of Mg-Fe-Mn-Li amphiboles. The cummingtonite-grunerite series of amphiboles are monoclinic and in the system described by Leake (1997), have the general series formula

* E-mail: jree99@esc.cam.ac.uk

$(Mg,Fe^{2+},Mn,Li)_7Si_8O_{22}(OH)_2$ (Li <1.00). The term cummingtonite applies to compositions with $Mg/(Mg+Fe^{2+}) \geqslant 0.50$, grunerite being the Fe^{2+}-rich end-member. The solid-solution end-members (Mn_2Mg_5) and ($Mn_2Fe_5^{2+}$) correspond to manganocummingtonite and manganogrunerite respectively. Cummingtonite occurs as polymorphs with space groups $C2/m$ and $P2_1/m$ with a phase transition occurring at relatively low temperatures for all natural compositions. Figure 1 shows the structure of a cummingtonite viewed parallel to (100).

Following reports (Bown, 1966) of a primitive structure in a Mg-rich Fe-Mg-Mn amphibole, Ross *et al.* (1968) suggested the possibility of the phase transition by analogy of $P2_1/m$ cummingtonite with pigeonite (and its $P2_1/c$–$C2/c$ transition). The $P2_1/m$ structure is only observed in Fe-Mg-Mn amphiboles and is restricted to those where Mg occupies 70–90% of B sites (Maresch and Czank, 1988). Upon substitution of Mn^{2+} and Fe^{2+} for the smaller Mg^{2+}, the crystal structure is forced to revert to $C2/m$ symmetry. Yang and Smyth (1996) provide evidence that the effective size of the M(4) cation controls the stability of the $C2/m$ and $P2_1/m$ structures. Yang and Hirschmann (1995) reported a compositional dependence of the transition such that, at room temperature, cummingtonite with $X_{Mg}^{M4} > 0.15 \pm 0.02$ will have $P2_1/m$ crystal structure. They also found ferromagnesian cummingtonite to be more stable in the $P2_1/m$ structure than manganoan cummingtonites with the same Mg-content. Also in this vein, Ghose and Ganguly (1982) found that cummingtonite with Fe/(Fe+Mg) = 0.22 has $P2_1/m$ symmetry. Hirschmann *et al.* (1994) reported $P2_1/m$ symmetry at room temperature in heat-treated cummingtonites which had Fe/(Fe+Mg) as high as 0.38. Samples as iron-rich as Fe/(Fe+Mg) = 0.45 are also $P2_1/m$ (Ross *et al.*, 1969). Sueno *et al.* (1972) studied the $P2_1/m$–$C2/m$ phase transition by *in situ* high-temperature X-ray diffraction (XRD), following the disappearance of the 102 reflection of the $(h + k = 2n + 1)$ set, representative of the primitive symmetry. They report a T_c of 100°C. The ferromagnesian cummingtonite investigated by Yang and Smyth (1996) shows a transition temperature of ~ −30°C.

Ordering of cations occurs in the octahedral strip, which represents the body of the 'I-beam' module in amphiboles and comprises three unique cation sites. In $C2/m$ cummingtonite there are three pseudo-octahedral sites, M(1), M(2) and M(3) with point symmetry 2, 2 and $2/m$ respectively. The M(4) cation site sits at the edge of the octahedral strip. This site is surrounded by eight anions and has point symmetry 2. The coordination of the site varies with cation occupancy. The octahedral strip in $P2_1/m$ cummingtonite also contains three pseudo-octahedral cation sites but the M(1) and M(2) sites have point symmetry 1 and M(3) has point symmetry *m*. The general position and coordina-

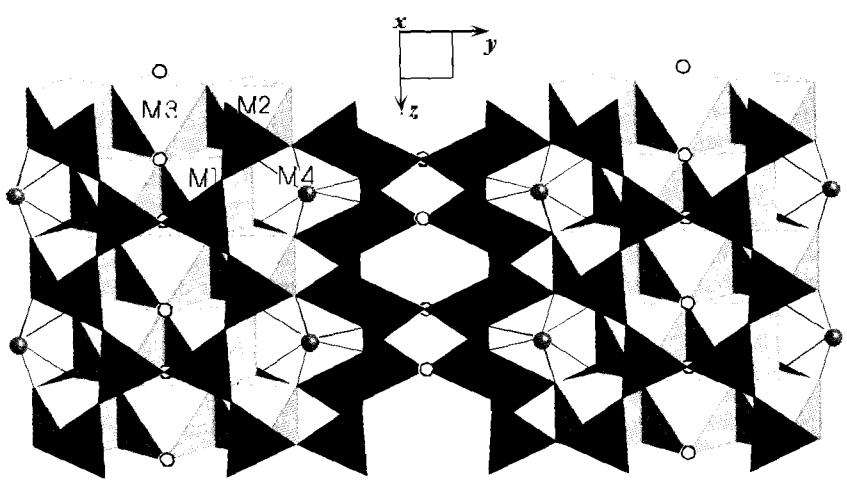

FIG. 1. View down [100] of the cummingtonite structure, showing the M(1), M(2) and M(3) sites in the octahedral ribbon with adjacent M(4). Open circles show the positions of hydroxyls.

tion of the M(4) site is the same as for the *C*2/*m* structure but it has point symmetry 1 (Leake, 1997; Hawthorne, 1983).

We are focusing on metal cation partitioning between the M(4) site and the smaller octahedral sites M(1), M(2) and M(3). Whittaker (1949) showed that, in crocidolite, Mg^{2+} occupies the M(4) cation site in preference to Fe^{2+}. Ten years later using three dimensional least squares refinement of XRD data from a grunerite, Ghose and Hellner (1959) reported almost complete occupation of the M(4) site by Fe^{2+} and showed that surplus Fe^{2+} and Mg^{2+} were distributed randomly over the three remaining cation sites. Ghose (1961) determined the crystal structure of a cummingtonite from Quebec with particular interest paid to cation distribution and disordering. Work on Fe-Mg ordering in a cummingtonite by Hirschmann *et al.* (1994) revealed a strong preference of Fe^{2+} for the M(4) site relative to Mg. However, the first to recognize the potential of cummingtonite as a geothermometer were Ghose and Weidner (1972). Using basic principles of geothermometry that had previously been applied to pyroxenes with limited success (Mueller, 1970) and recognizing the similarity in composition, structure and order-disorder mechanisms in orthopyroxene and cummingtonite, they determined a system of temperature dependent cation ordering of Mg^{2+} and Fe^{2+} between the M(4) and M(1,2,3) sites.

Ghose and Yang (1989) refined the crystal structure and determined the cation distribution of a *C*2/*m* manganoan cummingtonite from Nsuta, Ghana. On the basis of bond-lengths they reported that the sequence of site preference of Mn^{2+} in the Mn-Mg amphibole is M(4)≫M(1)>M(2)>M(3) and put the compositional limit for the $P2_1/m$ to *C*2/*m* phase transition at ambient temperatures close to $Mn_2Mg_5Si_8O_{22}(OH)_2$. However, the kinetics of cation exchange are not fully understood and are largely unconstrained. Furthermore, what is known of cation ordering in amphiboles has been determined from room temperature studies in anneal and quench experiments, the underlying assumption being that equilibrium states are attained during annealing and retained during quenching. Recent studies of cation ordering in spinels and olivines have shown that the kinetics of re-ordering may be very rapid (Redfern *et al.*, 1999). The possibility of rapid re-equilibration during quenching and the details of the kinetic pathways away from equilibrium remain unaddressed.

In order to determine the high-*T* equilibrium behaviour and the non-equilibrium kinetics of cation ordering, we have undertaken *in situ* crystallographic studies of an iron-free manganoan cummingtonite from Talcville, New York (Ross *et al.*, 1969), using time of flight, neutron powder diffraction techniques.

Experimental procedure

Approximately 5 g of sample R14473 of natural Talcville cummingtonite of composition $^{[M4]}(Na_{0.13}Ca_{0.41}Mg_{0.46}Mn_{1.00})$ $^{[M1,2,3]}(Mg_{4.87}Mn_{0.13})[Si_8O_{22}](OH)_2$ was used for neutron diffraction experiments. The composition of the cummingtonite was calculated by averaging electron microprobe analyses, normalized to 24 oxygens, of 20 separate crystals. The analyses were performed on a Cameca SX50 electron micro-probe. The sample was placed into a vanadium furnace inside the sample chamber of the POLARIS neutron powder diffractometer (Hull *et al.*, 1992). The sample chamber was evacuated to a pressure of 10^{-6}mbar. The sample was heated in increments of 50°C to a maximum of 700°C and assumed to have reached thermal equilibrium after ten minutes at each temperature plateau. Powder diffraction patterns were then collected over a period of 4–5 h at each temperature with 58 ^{3}He gas tube detectors positioned at $2\theta = 145°$ and 216 ZnS detectors at $2\theta = 90°$. On cooling, further diffraction patterns were collected at temperatures of 500, 350 and 200°C. All diffraction patterns were refined using whole pattern fitting using the Rietveld method (Rietveld, 1969). This method was recently employed to study A-site partitioning in amphibole using X-ray diffraction (Sokolova *et al.*, 2000). The structures were refined in space group *C*2/*m* ($Z = 2$) for experiments at all temperatures. The background was refined using ten coefficients of a Chebyshev function. The site occupancies of Mg^{2+} and Mn^{2+} on the M(1), M(2), M(3) and M(4) site were refined using chemical constraints. Neutron scattering lengths for all atoms were those given by Sears (1992). The starting model for the refinement used initial atomic coordinates from Sueno *et al.* (1972) and constrained all Mn to either the M(2) or M(4) sites after our previous unconstrained refinements yielded this result. Convergence of the least squares cycle was achieved for each refinement. R_{wp} factors of ~2% were achieved

TABLE 1. Refined structural parameters as a function of temperature. Figures in parentheses represent the estimated standard deviation. H(1)*y*, O(3) *y*, O(7)*y*, M(1)*x*, M(2)*x*, *z*, M(4)*x* and M(3)*x*,*y*,*z* are all 0. M(1)*z* and M(4)*z* are ½. H(1)*y*, O(3) *y*, O(7)*y*, M(1)*x*, M(2)*x*,*z*, M(4)*x* and M(3)*x*,*y*,*z* are all 0. The fractional site occupancies of Na and Ca on M(4) are 0.065 and 0.205 respectively.

Atom position	Temperature (°C) 50	100	150	200	250	300	350	400	450	500	550	600	650	700	500	350	200
H(1)																	
x	0.2212(13)	0.2215(13)	0.2224(14)	0.2225(15)	0.2239(16)	0.2241(16)	0.2275(17)	0.2261(18)	0.2263(18)	0.2277(19)	0.2257(21)	0.2235(22)	0.2269(23)	0.2265(23)	0.2255(20)	0.2264(17)	0.2228(14)
z	0.7381(23)	0.7481(24)	0.7386(25)	0.7377(27)	0.7368(29)	0.7362(29)	0.7269(31)	0.7287(33)	0.7269(33)	0.723(4)	0.720(4)	0.718(4)	0.715(4)	0.718(4)	0.725(4)	0.7335(31)	0.7417(26)
Uiso	4.68(27)	5.25(28)	6.05(32)	6.9(4)	7.7(4)	8.6(4)	9.3(5)	10.5(5)	10.6(5)	11.5(6)	12.2(6)	12.6(7)	13.3(7)	13.9(8)	11.4(6)	9.4(5)	6.96(35)
O(1)																	
x	0.1164(4)	0.1168(4)	0.1168(4)	0.1169(4)	0.1168(4)	0.1169(4)	0.1170(4)	0.1169(4)	0.1169(4)	0.1171(4)	0.1169(4)	0.1166(4)	0.1167(4)	0.1169(4)	0.1166(4)	0.1166(4)	0.1166(4)
y	0.0877(2)	0.0876(2)	0.0877(2)	0.0879(2)	0.0879(2)	0.0878(2)	0.0878(2)	0.0877(2)	0.0878(2)	0.0877(2)	0.0880(2)	0.0879(2)	0.0880(2)	0.0877(2)	0.0878(2)	0.0876(2)	0.0875(2)
z	0.2154(7)	0.2146(7)	0.2153(7)	0.2155(8)	0.2157(8)	0.2145(8)	0.2159(8)	0.2146(8)	0.2146(8)	0.2146(8)	0.2163(9)	0.2161(9)	0.2163(9)	0.2147(9)	0.2158(9)	0.2146(8)	0.2142(7)
Uiso	0.475(16)	0.479(16)	0.537(16)	0.592(16)	0.650(17)	0.666(17)	0.816(19)	0.766(18)	0.823(19)	0.883(19)	1.004(21)	1.062(21)	1.140(22)	1.132(23)	0.951(20)	0.761(18)	0.568(16)
O(2)																	
x	0.1215(4)	0.1215(4)	0.1217(4)	0.1217(4)	0.1217(4)	0.1215(4)	0.1214(4)	0.1214(4)	0.1213(4)	0.1210(4)	0.1212(4)	0.1213(4)	0.1209(4)	0.1207(4)	0.1215(4)	0.1215(4)	0.1217(3)
y	0.1727(2)	0.1726(2)	0.1726(2)	0.1726(2)	0.1727(2)	0.1728(2)	0.1727(2)	0.1728(2)	0.1729(2)	0.1729(2)	0.1727(2)	0.1727(2)	0.1728(2)	0.1730(2)	0.1727(2)	0.1729(2)	0.1728(2)
z	0.7182(7)	0.7188(7)	0.7190(7)	0.7190(7)	0.7190(7)	0.7187(10)	0.7186(8)	0.7188(8)	0.7188(8)	0.7188(8)	0.7186(8)	0.7190(9)	0.7189(9)	0.7185(9)	0.7187(8)	0.7184(8)	0.7186(7)
Uiso	0.475(1)	0.479(2)	0.537(16)	0.592(16)	0.650(17)	0.666(17)	0.816(19)	0.766(18)	0.823(19)	0.883(19)	1.004(21)	1.062(21)	1.140(22)	1.132(23)	0.951(20)	0.761(18)	0.568(16)
O(3)																	
x	0.1041(5)	0.1040(5)	0.1039(5)	0.1041(5)	0.1037(5)	0.1030(5)	0.1035(5)	0.1028(5)	0.1029(5)	0.1021(5)	0.1034(5)	0.1037(6)	0.1038(6)	0.1032(6)	0.1039(6)	0.1032(5)	0.1035(5)
z	0.7144(10)	0.7139(10)	0.7141(10)	0.7140(10)	0.7143(10)	0.7151(10)	0.7145(11)	0.7155(10)	0.7155(11)	0.7158(11)	0.7149(12)	0.7146(12)	0.7142(12)	0.7142(12)	0.7148(12)	0.7152(10)	0.7142(10)
Uiso	0.475(16)	.0479(116)	0.537(16)	0.592(16)	0.650(17)	0.666(17)	0.816(19)	0.766(18)	0.823(19)	0.883(19)	1.004(21)	1.062(21)	1.140(22)	1.132(23)	0.951(20)	0.761(18)	0.568(16)
O(4)																	
x	0.3773(4)	0.3768(36)	0.3774(4)	0.3776(4)	0.3773(4)	0.3766(4)	0.3779(4)	0.3766(4)	0.3768(4)	0.3765(4)	0.3775(4)	0.3775(4)	0.3775(4)	0.3770(4)	0.3775(4)	0.3768(4)	0.3768(4)
y	0.2467(2)	0.2470(2)	0.2471(2)	0.2469(2)	0.2468(2)	0.2466(2)	0.2463(2)	0.2464(2)	0.2462(2)	0.2461(2)	0.2459(2)	0.2457(2)	0.2455(2)	0.2453(2)	0.2458(2)	0.2463(2)	0.2467(2)
z	0.7812(8)	0.7817(7)	0.7828(8)	0.7831(8)	0.7833(8)	0.7832(8)	0.7839(8)	0.7387(8)	0.7837(8)	0.7834(8)	0.7838(9)	0.7838(9)	0.7835(9)	0.7824(9)	0.7837(9)	0.7832(8)	0.7822(8)
Uiso	0.475(16)	0.479(16)	0.537(16)	0.592(16)	0.650(17)	0.666(17)	0.816(19)	0.766(18)	0.823(19)	0.883(19)	1.004(21)	1.062(21)	1.140(22)	1.132(23)	0.951(20)	0.761(18)	0.568(16)
O(5)																	
x	0.3472(4)	0.3469(4)	0.3460(4)	0.3450(4)	0.3449(4)	0.3443(4)	0.3436(4)	0.3431(4)	0.3429(4)	0.3426(4)	0.3419(4)	0.3417(4)	0.3415(4)	0.3420(4)	0.3420(4)	0.3433(4)	0.3447(3)
y	0.1289(2)	0.1292(2)	0.1291(2)	0.1288(2)	0.1285(2)	0.1284(2)	0.1281(2)	0.1281(2)	0.1280(2)	0.1278(2)	0.1275(2)	0.1273(2)	0.1270(2)	0.1269(2)	0.1276(2)	0.1281(2)	0.1289(2)
z	0.0596(6)	0.0605(6)	0.0600(6)	0.0590(6)	0.0588(6)	0.0588(6)	0.0572(6)	0.0578(6)	0.0576(6)	0.0565(6)	0.0552(6)	0.0551(7)	0.0538(7)	0.0540(7)	0.0553(6)	0.0573(6)	0.0589(6)
Uiso	0.475(16)	0.479(16)	0.537(16)	0.592(16)	0.650(17)	0.666(17)	0.816(19)	0.766(18)	0.823(19)	0.883(19)	1.004(21)	1.062(21)	1.140(22)	1.132(23)	.0951(20)	0.761(18)	0.568(16)
O(6)																	
x	0.3542(3)	0.3540(3)	0.3543(3)	0.3553(3)	0.3558(3)	0.3561(3)	0.3566(3)	0.3575(3)	0.3577(3)	0.3578(3)	0.3581(4)	0.3587(4)	0.3586(4)	0.3586(4)	0.3584(4)	0.3571(3)	0.3557(3)
y	0.1202(2)	0.1209(2)	0.1211(2)	0.1212(2)	0.1212(2)	0.1210(2)	0.1213(2)	0.1212(2)	0.1212(2)	0.1211(2)	0.1214(2)	0.1212(2)	0.1213(2)	0.1211(2)	0.1213(2)	0.1212(2)	0.1213(2)
z	0.5695(6)	0.5686(6)	0.5670(6)	0.5668(6)	0.5666(6)	0.5671(6)	0.5666(6)	0.5664(6)	0.5661(6)	0.5660(6)	0.5653(6)	0.5650(6)	0.5645(7)	0.5648(7)	0.5646(6)	0.5658(6)	0.5662(6)
Uiso	0.475(16)	0.479(16)	0.537(16)	0.592(16)	0.650(17)	0.666(17)	0.816(19)	0.766(18)	0.823(19)	0.883(19)	1.004(21)	1.062(21)	1.140(22)	1.132(23)	0.951(20)	0.761(18)	0.568(16)
O(7)																	
x	0.3403(4)	0.3404(4)	0.3401(4)	0.3396(4)	0.3394(5)	0.3392(4)	0.3381(5)	0.3384(5)	0.3378(5)	0.3376(5)	0.3359(5)	0.3358(5)	0.3352(5)	0.3356(5)	0.3365(5)	0.3388(5)	0.3400(4)

TABLE 1. (*Contd.*)

Atom position	Temperature (°C) 50	100	150	200	250	300	350	400	450	500	550	600	650	700	500	350	200
z	0.2781(8)	0.2767(8)	0.2567(8)	0.2757(8)	0.2758(8)	0.2764(8)	0.2766(8)	0.2763(9)	0.2768(8)	0.2773(9)	0.2772(9)	0.2775(9)	0.2782(10)	0.2785(10)	0.2766(9)	0.2759(8)	0.2759(8)
Uiso	0.475(16)	0.479(16)	0.537(16)	0.592(16)	0.650(17)	0.666(17)	0.816(19)	0.766(18)	0.823(19)	0.883(19)	1.004(21)	1.062(21)	1.140(22)	1.132(23)	0.951(20)	0.761(18)	0.568(16)
Si(1)																	
x	0.2845(5)	0.2852(4)	0.2852(5)	0.2855(5)	0.2858(5)	0.2866(5)	0.2873(5)	0.2876(5)	0.2874(5)	0.2881(5)	0.2877(5)	0.2873(5)	0.2885(6)	0.2886(6)	0.2873(5)	0.2867(5)	0.2857(5)
y	0.0849(2)	0.0847(2)	0.0848(2)	0.0849(2)	0.0851(2)	0.0852(2)	0.0852(2)	0.0855(2)	0.0855(2)	0.0856(2)	0.0857(3)	0.0859(3)	0.0859(3)	0.0860(3)	0.0859(3)	0.0855(2)	0.0852(2)
z	0.2759(8)	0.2767(8)	0.2761(8)	0.2768(8)	0.2768(9)	0.2774(8)	0.2767(9)	0.2776(9)	0.2779(9)	0.2778(9)	0.2776(9)	0.2779(10)	0.2779(10)	0.2784(10)	0.2773(9)	0.2768(9)	0.2770(8)
Uiso	0.207(31)	0.212(30)	0.275(31)	0.301(31)	0.332(31)	0.339(31)	0.469(33)	0.384(32)	0.420(32)	0.437(33)	0.55(4)	0.61(4)	0.61(4)	0.60(4)	0.52(4)	0.414(32)	0.291(30)
Si(2)																	
x	0.2930(5)	0.2922(5)	0.2922(5)	0.2920(5)	0.2916(5)	0.2903(5)	0.2899(5)	0.2892(5)	0.2891(5)	0.2883(5)	0.2893(5)	0.2895(5)	0.2884(6)	0.2873(6)	0.2899(5)	0.2901(5)	0.2914(5)
y	0.1685(2)	0.1689(2)	0.1691(2)	0.1689(23)	0.1688(2)	0.1688(2)	0.1687(2)	0.1690(2)	0.1687(2)	.01689(2)	0.1683(3)	0.1682(3)	0.1680(3)	0.1681(3)	0.1684(3)	0.1687(2)	0.1688(2)
z	0.7823(8)	0.7816(8)	0.7816(8)	0.7813(8)	0.7810(8)	0.7805(8)	0.7801(9)	0.7799(8)	0.7797(9)	0.7796(9)	0.7798(9)	0.7801(9)	0.7796(10)	0.7792(10)	0.7795(9)	0.7796(8)	0.7802(8)
Uiso	0.207(31)	0.212(30)	0.275(31)	0.301(31)	0.332(31)	0.339(31)	0.469(33)	0.384(32)	0.420(32)	0.437(33)	0.55(4)	0.61(4)	0.61(4)	0.60(4)	0.52(4)	0.414(32)	0.291(30)
M(1)																	
y	0.0870(3)	0.0871(3)	0.0873(3)	0.0874(3)	0.0874(3)	0.0873(3)	0.0875(3)	0.0875(3)	0.0875(3)	0.0875(3)	0.0877(3)	0.0877(3)	0.0877(3)	0.0874(3)	0.08751(3)	0.08735(3)	0.0872(3)
Uiso	0.088(32)	0.165(32)	0.220(33)	0.280(34)	0.36(4)	0.44(4)	0.59(4)	0.62(4)	0.70(4)	0.80(4)	0.92(4)	1.07(5)	1.23(5)	1.29(5)	0.95(4)	0.64(4)	0.342(34)
M(2)																	
y	0.1755(3)	0.1760(3)	0.1761(3)	0.1763(3)	0.1764(3)	0.1766(3)	0.1763(3)	0.1766(3)	0.1767(3)	0.1766(3)	0.1765(3)	0.1767(3)	0.1765(3)	0.1767(4)	0.1766(3)	0.1767(3)	0.1767(3)
Uiso	0.088(32)	0.165(32)	0.220(33)	0.280(34)	0.36(4)	0.44(4)	0.59(4)	0.62(4)	0.70(4)	0.80(4)	0.92(4)	1.07(5)	1.23(5)	1.29(5)	0.95(4)	0.64(4)	0.342(34)
Mn Frac.	0.067(6)	0.065(5)	0.065(6)	0.066(6)	0.063(6)	0.063(6)	0.067(6)	0.062(6)	0.063(6)	0.060(6)	0.057(6)	0.060(7)	0.068(7)	0.078(7)	0.076(6)	0.082(6)	0.083(6)
Mg Frac.	0.933(6)	0.935(5)	0.935(6)	0.934(6)	0.937(6)	0.937(6)	0.933(6)	0.938(6)	0.937(6)	0.940(6)	0.943(6)	0.940(7)	0.932(7)	0.922(7)	0.924(6)	0.918(6)	0.917(6)
M(3)																	
Uiso	0.088(32)	0.165(32)	0.220(33)	0.280(34)	0.36(4)	0.44(4)	0.59(4)	0.62(4)	0.70(4)	0.80(4)	0.92(4)	1.07(5)	1.23(5)	1.29(5)	0.95(4)	0.64(4)	0.342(34)
M(4)																	
y	0.2369(22)	0.2375(22)	0.2362(22)	0.2356(22)	0.2375(25)	0.2423(24)	0.2396(24)	0.2453(26)	0.2459(26)	0.2479(29)	0.2438(32)	0.2469(31)	0.2496(28)	0.2542(24)	0.2483(24)	0.2484(20)	0.2441(18)
Uiso	0.088(32)	0.165(32)	0.220(33)	0.280(34)	0.36(4)	0.44(4)	0.59(4)	0.62(4)	0.70(4)	0.80(4)	0.92(4)	1.07(5)	1.23(5)	1.29(5)	0.95(4)	0.64(4)	0.342(34)
Mn Frac.	0.503(6)	0.505(5)	0.505(6)	0.504(6)	0.508(6)	0.507(6)	0.504(6)	0.508(6)	0.507(6)	0.510(6)	0.513(6)	0.510(7)	0.502(7)	0.493(7)	0.494(6)	0.489(6)	0.487(6)
Mg Frac.	0.227(6)	0.225(5)	0.225(6)	0.226(6)	0.222(6)	0.223(6)	0.226(6)	0.222(6)	0.223(6)	0.220(6)	0.217(6)	0.220(7)	0.228(7)	0.237(7)	0.236(6)	0.241(6)	0.243(6)
a (Å)	9.5539(2)	9.5566(2)	9.5611(2)	9.5661(2)	9.5714(2)	9.5761(2)	9.5824(2)	9.5876(2)	9.5933(2)	9.5994(2)	9.6061(2)	9.6120(2)	9.6182(2)	9.6236(2)	9.6004(2)	9.5823(2)	9.5663(2)
b (Å)	18.0293(3)	18.0373(3)	18.0458(3)	18.0531(3)	18.0610(3)	18.0678(3)	18.0767(3)	18.0841(3)	18.0925(3)	18.1008(3)	18.1101(3)	18.1206(4)	18.1323(4)	18.1425(4)	18.1087(3)	18.0835(3)	18.0607(3)
c (Å)	5.2999(1)	5.3034(1)	5.3056(1)	5.3069(1)	5.3082(1)	5.3089(1)	5.3104(1)	5.3113(1)	5.3124(1)	5.3135(1)	5.3151(1)	5.3166(1)	5.3185(1)	5.3198(1)	5.3152(1)	5.3113(1)	5.3080(1)
β (°)	102.614(2)	102.592(2)	102.569(2)	102.549(2)	102.529(2)	102.511(2)	102.493(2)	102.475(2)	102.457(2)	102.440(2)	102.422(2)	102.397(2)	102.363(2)	102.335(2)	102.404(2)	102.454(2)	102.511(2)
R_{wp}	0.0258	0.0214	0.0207	0.0194	0.0194	0.0193	0.0182	0.0176	0.0171	0.0168	0.0165	0.0162	0.016	0.0161	0.0172	0.0182	0.021

for profiles obtained for the detector banks at 90° and 145°2θ. Here, R_{wp}, the R-weighted profile is used to assess the quality of the refinement since the numerator is the residual of the fit. It is defined as:

$$R_{wp} = \left[\frac{\sum_i w_i(I_i - I_{i,calc})^2}{\sum_i w_i I_i^2}\right]^{1/2}$$

where I_i and $I_{i,calc}$ are the observed and calculated intensities at the i^{th} point in the pattern respectively and the weighting, w_i is related to the estimated standard deviation in the intensity of the i^{th} point by $w_i = 1/\sigma_i^2$.

An infrared powder absorption spectrum of the sample was recorded at room temperature in the wavenumber region 500–4500 cm^{-1} (Boffa Ballaran, unpublished data) using a Bruker 67V FT-IR spectrometer. The sample was prepared as a pressed pellet, diluted to 0.29 wt.% of the CsI pellet.

Results

Table 1 displays the refined structural parameters of sample R14473 as a function of temperature. Also shown are the R factors for each refinement.

A graphical representation of the refined time-of-flight neutron diffraction pattern for sample R14473 at 650°C is given in Fig. 2. Also shown is the minimized difference in fit line, giving the difference between observed diffraction pattern and that refined using the GSAS program by Larson and Von Dreele (1994). The consequent structural formula obtained after refinement of the low temperature (50°C) diffraction pattern is $^{[M4]}(Na_{0.13}Ca_{0.41}Mg_{0.46}Mn_{1.00})$ $^{[M1,2,3]}(Mg_{4.87}Mn_{0.13})[Si_8O_{22}](OH)_2$. The presence of Na^+ substituted for Ca^{2+} in M(4) suggests that, of the Mn, 0.13 per formula unit is Mn^{3+}. However, the amount of Na^+ recorded in the microprobe analyses ($\approx 0.3-0.4\%$ element) is only just above the levels of detection of the instrument and therefore the presence of Mn^{3+} must be accepted with caution.

The exchange reaction of Mn^{2+} and Mg^{2+} between the M(4) and M(2) sites, has the equilibrium constant:

$$K_D = \frac{Mn^{M(4)}(1 - Mn^{M(2)})}{Mn^{M(2)}(1 - Mn^{M(4)})}$$

Therefore, a value of $K_D = 1$ would represent complete disorder between M(4) and M(2), $K_D = 0$

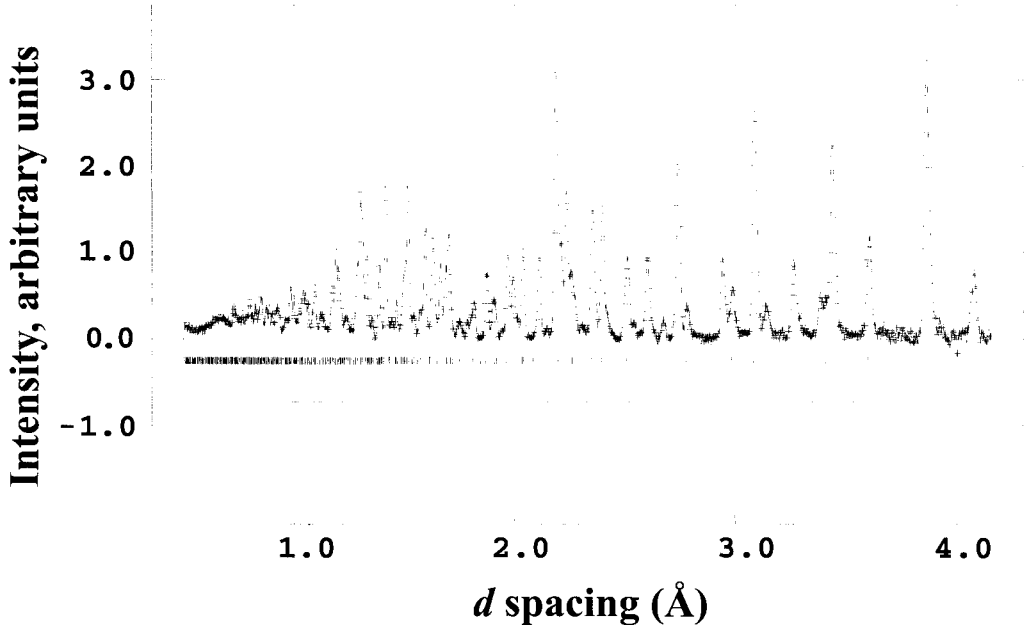

FIG. 2. The time-of-flight neutron powder diffraction pattern of cummingtonite R14473 at 650°C. The vertical markers show the calculated positions of reflections and the Rietveld fit is shown by the solid line. Also shown is the residual between calculated pattern and the pattern determined by experiment.

corresponds to complete anti-order and $K_D = \infty$ would imply complete order.

There is a suggestion of an initial increase in the occupancy of the M(4) site by Mn^{2+} (see Fig. 3) until a temperature of ~550°C, at which point a sharp decline in X_{Mn}^{M4} commences and K_D decreases from a maximum of 17.4 to a minimum of 11.5 on heating, corresponding to disordering. Another interesting feature of Fig. 3 is the retention of the high-temperature disorder on cooling. Our results show that exchange is predominantly between M(4) and M(2). Alternative refinements, constraining all Mn to the M(4) site at lower temperatures, produced negative isotropic temperature factors. Once unconstrained, these models immediately converged upon site occupancies identical to those of the M(4)–M(2) model with the same R_{wp}s and temperature factors. Additional models that constrained all Mn to just the M(4) and M(1) sites were also found to be erroneous and unstable.

The distribution coefficient, K_D, is related to the Gibbs free energy for the exchange of cations, as follows:

$$\Delta G = -RT\ln K_D$$

where ΔG is the Gibbs free energy of disorder and T is the absolute temperature. The data from the three highest temperatures were used to determine this exchange energy as these represent equilibrium conditions, and gave an exchange energy of 24.6 ± 1.5 kJ mol^{-1}.

The cell parameters of our sample (Fig. 4) show linear relationships with increasing temperature, but in two or three segments. The a and b lattice parameters both show two stages or rates of expansion on heating, the a parameter strain behaviour showing a 'kink' at roughly 150°C and the b parameter expansion rate increases at 500–550°C. The strain behaviour of the c parameter on heating may be divided into three linear portions, the nodes of which coincide with the temperatures at which the change in rate of expansion occurs in the a and b parameters. At the higher of the two temperatures, marked changes in the β angle and the volume of the unit cell (Fig. 4) also occur. It is also noticeable that on cooling, a displacement of all parameters except a is maintained.

Figure 5 shows the positional behaviour of the hydrogen atom within the structure upon heating and cooling. The decrease in z and increase in x above 100°C are the result of the $P2_1/m$ to $C2/m$ phase transition. The behaviour of the hydrogen atom as a direct result of the onset of disordering at ~550°C cannot be defined within the errors illustrated. The *in situ* results do show that during cooling of the sample, the hydrogen atom returns to the positions it originally occupied (within error) at the respective temperatures during heating.

The infrared spectrum of the amphibole (Fig. 6) has a strong sharp peak centred at 3670 cm^{-1} with a small shoulder at 3674 cm^{-1}. The main peak corresponds to an O(3) cation triplet MgMgMg

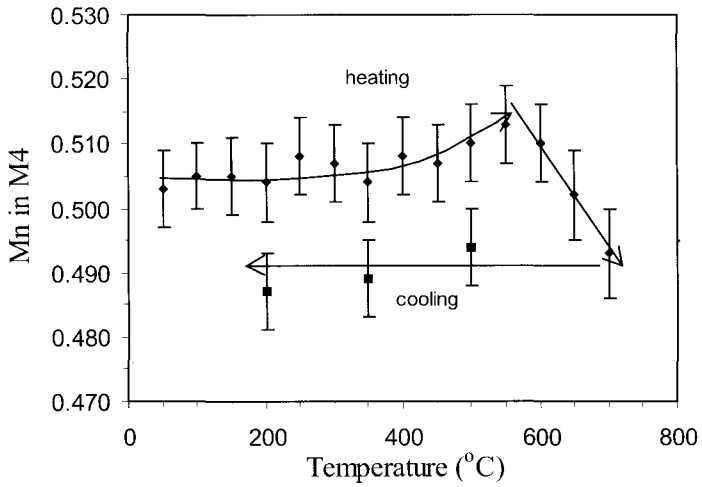

FIG. 3. Mn^{2+} occupancy of the M(4) site. Note the 'frozen in' disordered state during cooling.

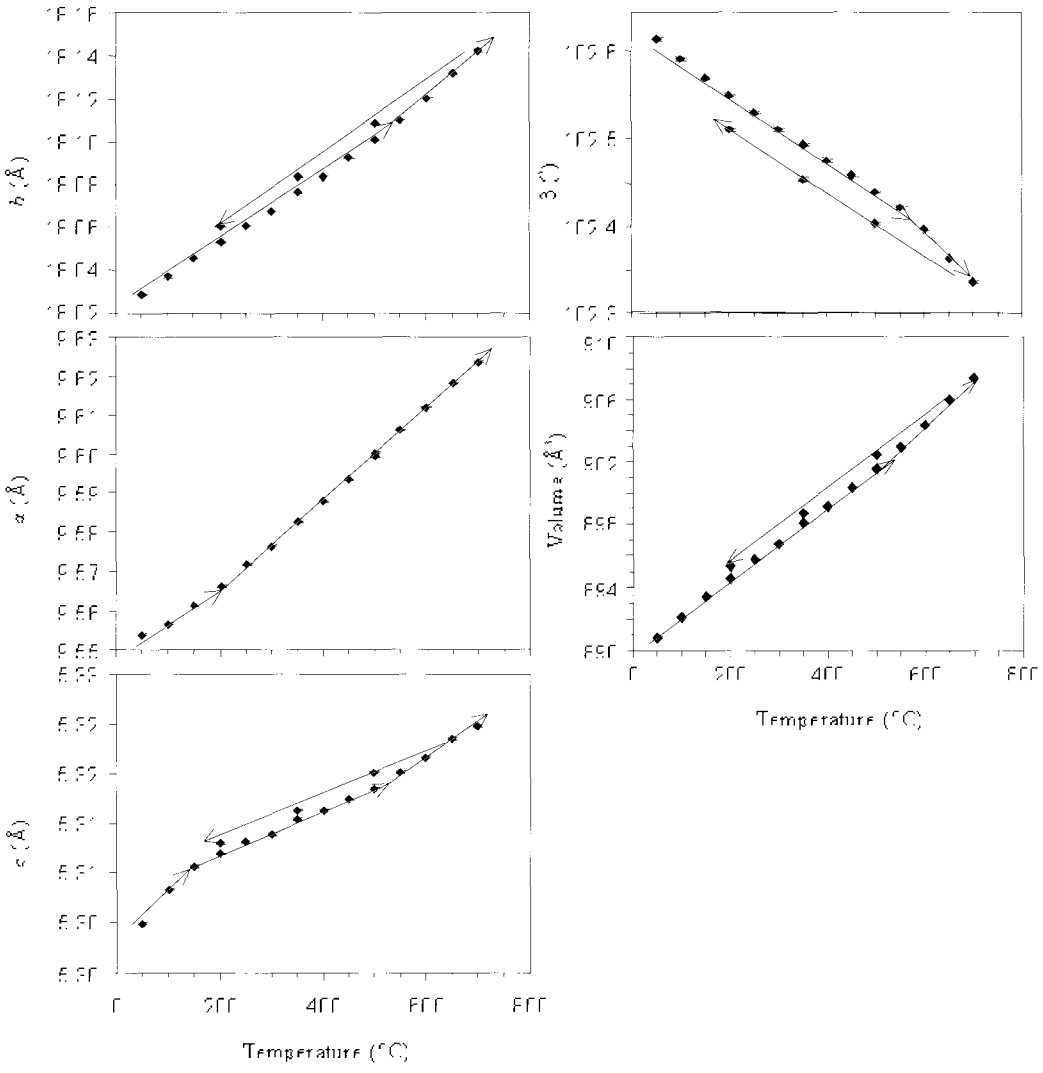

FIG. 4. Cell parameters and volume as a function of temperature.

(Burns and Strens, 1966), consistent with complete occupancy of M(1) and M(3) sites by Mg. Subtle splitting of main absorption bands has been observed in amphiboles with mixed M(4) site occupancy. In a slightly synthetic tremolite with minor Mg at M(4), Hawthorne *et al.* (1996) observed a small shoulder at ~3670 cm^{-1} due to $MgMgMg/^{M(4)}Mg$ in addition to the strong main peak at 3674 cm^{-1} due to $MgMgMg/^{M(4)}Ca$. Thus, for the Talcville cummingtonite (with Mn as the main M(4) cation), it seems reasonable to ascribe the main absorption at 3670 cm^{-1} to $MgMgMg/^{M(4)}Mn$ (and $^{M(4)}Mg$?) and the peak at 3674 cm^{-1} to $MgMgMg/^{M(4)}Ca$, in line with the assignments of Burns and Strens (1966) and Hawthorne *et al.* (1996). Mn substitution for Mg at M(1) and/or M(3) would, by analogy with Fe^{2+} for Mg (Burns and Strens, 1966), be expected to lead to peaks at frequencies 15–20 cm^{-1} lower than those due to MgMgMg, and so we can be confident that the 3674 cm^{-1} peak is not due to Mn at M(1) and/or M(3).

Table 2 lists some octahedral bond lengths in the structure at 750, 250 and 50°C. Also listed are

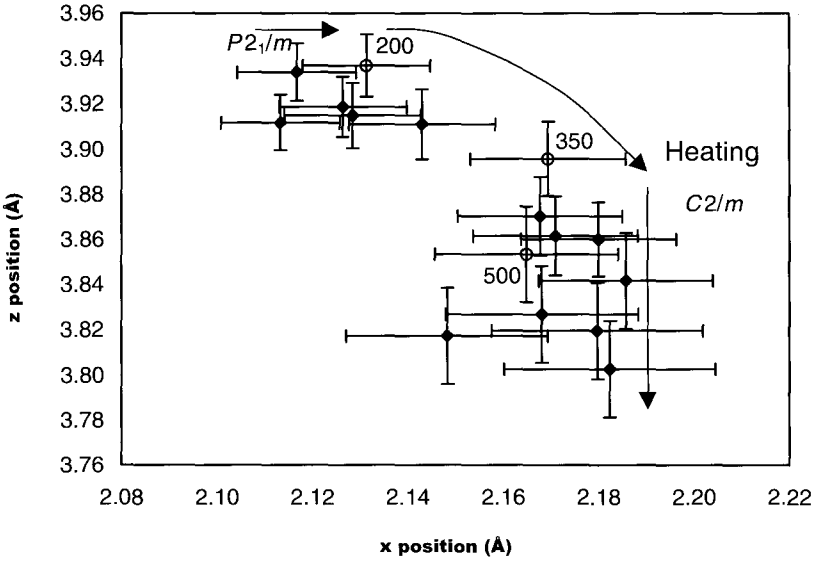

FIG. 5. The positional behaviour of the hydrogen atoms within the unit cell as a function of temperature. The open circles represent the position at the temperatures labelled during cooling.

the same bond lengths as reported by Sueno *et al.* (1972), for the same structure. Our results for bonds to M(4) are subject to a relatively high error, due to the low total scattering length of the M(4) site, where positive scattering (principally from Ca which has b = +4.70 fm, but also from Mg and Na) is reduced by the large negative scattering contribution from Mn (b = −3.73 fm). This means that the positional error on M(4) is high. Papike *et al.* (1969) noted that in cummingtonites, when the M(4) site is occupied by Fe and Mn, the O(5) oxygens are lost outside the M(4) coordination sphere, the M(4) cations move in the *b* direction towards the octahedral strip. Our bond lengths show that this effect is even more exagerrated than previously thought and a covalency between M(4)–O(2) is confirmed by bond lengths considerably shorter than the sum of the ionic radii of Mn^{2+} and O^{2-}. This type of covalent bonding has already been reported on the basis of short M(4)–O(4) bonds in Mg-Mn amphiboles (Ghose and Yang, 1989). The M(4)–O(4) bonds given by our refinements also show a lesser degree of covalency. In the most disordered state we observed that the average M(4) cation position has moved parallel to [010], away from the octahedral strip, decreasing the degree of M(4)–O(2) covalent bonding.

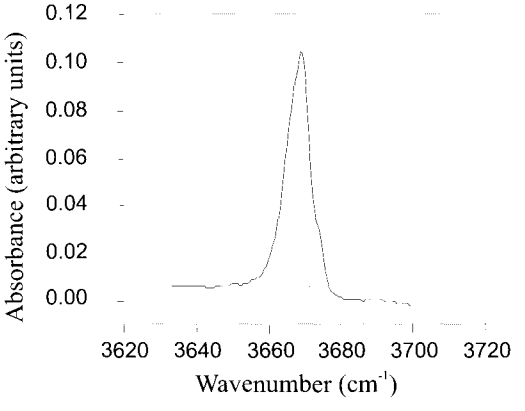

FIG. 6. Infra-red spectra showing the region containing the hydroxl stretching peak.

Discussion

The data presented show a definite preference of Mn^{2+} for the M(4) site with some disorder into the smaller M(2) site occurring at high temperature. It has been recognized previously (Ghose and Yang, 1989; Hawthorne and Grundy, 1977) that, in the absence of Fe^{2+}, the preference of Mn^{2+} for the M(2) site is greatly increased. This is confirmed in our results by the site preference sequence M(4)≫M(2)≫M(1,3), compared to that reported by Ghose and Yang

TABLE 2. Bond lengths as given by our refinements and those of Sueno *et al.* (1972). All bond lengths are in angstroms and figures represented in parentheses represent the error in the last digit of the bond length given.

Bond	This study			Sueno *et al.*, 1972
	750°C	250°C	50°C	270°C
M1–O1	2.073 (5)	2.064 (4)	2.060 (4)	2.063 (4)
M1–O2	2.130 (6)	2.121 (5)	2.118 (5)	2.112 (5)
M1–O3	2.077 (6)	2.069 (5)	2.062 (5)	2.087 (4)
<M1–O>	2.093	2.085	2.080	2.087
M2–O1	2.151 (7)	2.136 (5)	2.119 (5)	2.141 (5)
M2–O2	2.083 (4)	2.083 (4)	2.082 (4)	2.082 (4)
M2–O4	2.039 (6)	2.010 (5)	2.023 (5)	2.031 (5)
<M2–O>	2.091	2.076	2.075	2.085
M3–O1	2.134 (4)	2.126 (3)	2.117 (3)	2.089 (4)
M3–O3	1.986 (6)	1.984 (5)	1.984 (5)	2.059 (6)
<M3–O>	2.085	2.079	2.073	2.079
M4–O2	2.072 (32)	1.867 (28)	1.856 (25)	2.215 (4)
M4–O4	2.102 (5)	2.119 (7)	2.108 (6)	2.109 (5)
M4–O6	2.70 (4)	2.96 (4)	2.986 (33)	2.584 (5)
<M1–M1	3.169 (13)	3.156 (10)	3.139 (10)	3.147 (6)
M1–M2	3.115 (5)	3.103 (4)	3.093 (4)	3.109 (2)
M1–M3	3.096 (3)	3.087 (3)	3.079 (2)	3.085 (1)
M1–M4	3.03 (4)	2.71 (4)	2.70 (4)	3.202 (4)
M2–M3	3.206 (6)	3.186 (5)	3.164 (5)	3.195 (3)
M2–M4	3.008 (22)	2.873 (17)	2.873 (15)	3.089 (2)

(1989) of M(4)≫M(1)>M(2)>M(3) in a Mn-Mg cummingtonite with 0.15 Fe per formula unit. It seems likely that the absence of Fe in the Talcville sample allows the occupation of M(2) by Mn^{2+}, as indicated by our neutron refinements and room temperature infrared spectrum.

During heating, an initial increase in X_{Mn}^{M4} occurs as the amphibole adjusts towards the equilibrium Mn partitioning for these temperatures, until ~550°C, whereupon disordering into the smaller M(2) site becomes kinetically possible, showing a site preference energy of 24.6 ± 1.5 kJ mol^{-1}. Analogous 'relaxation' behaviour has been observed in olivines and spinels (Redfern *et al.*, 1996; Henderson *et al.*, 1996). This is a greater exchange energy than 8.95 kJ mol^{-1}, reported by Ghose and Yang (1989) for Fe-Mg exchange in an amphibole with $X^{Mn}/X^{Fe} = 0.378$ and than 18.33 kJ mol^{-1} found in Mn-Mg amphibole with $X^{Mn}/X^{Fe} = 0.350$. Hirschmann *et al.* (1994) reported an ordering energy of Fe-Mg between M(1) and M(4),($-RT\ln K_{1,4}$) of 18.2 ± 0.3 kJ mol^{-1}, in natural ferromagnesian clinoamphiboles with Fe/(Fe+Mg) as great as 0.38. They also reported a decrease in this ordering energy in very magnesian compositions but found the reaction to be otherwise independent of temperature over the range 600–750°C. The variation in quoted exchange energies may be due to differences in composition or oxygen fugacity at the temperatures of study. We note that our *in situ* experiments were conducted under very low oxygen fugacity, at the vanadium-vanadium oxide buffer. It is apparent that the disordered structural arrangements are retained during cooling of the sample.

The distortion in lattice parameters during heating above 100°C is interpreted as resulting from the $P2_1/m$ to $C2/m$ phase transition. The strain behaviour in the lattice parameters shows that the spontaneous strain resulting from the $P2_1/m \rightarrow C2/m$ transition is predominantly a shear with $+\varepsilon_1 \approx -\varepsilon_3$. Taking the data above 150°C as the paraphase (the high symmetry phase), we have calculated spontaneous strains of $\varepsilon_1 = 0.0734\%$ and $\varepsilon_3 = -0.0708\%$ at room temperature, which decrease in magnitude on heating to T_c. The scalar

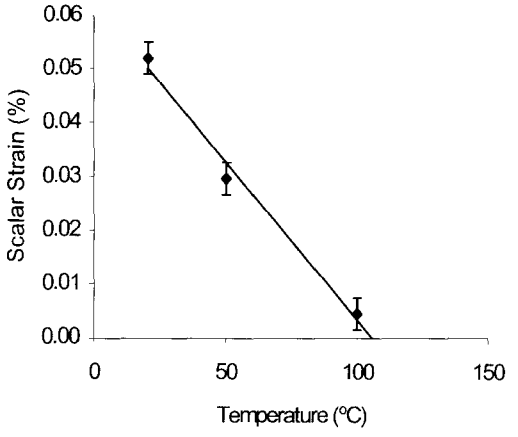

FIG. 7. Scalar strain as a function of temperature, falling to zero at the transition temperature of 107°C.

strain may be calculated as the geometric average of ε_1 and ε_3 and falls to zero at a T_c of 107°C. This T_c is higher than for the Fe-free cummingtonite also from the Talc district, New York, given by Prewitt *et al.* (1970), who reported a T_c of 45°C, but is comparable to the figure of Sueno *et al.* (1972) who give a T_c of 100°C (Fig. 7). In their samples, all but the *c* parameter, were greater than the cell parameters refined here. From our limited data, the spontaneous strain appears to be linearly dependent on temperature below T_c. Since, for this transition, strain must behave as the square of the order parameter (the transition is a zone-boundary instability) this indicates that the $P2_1/m \rightarrow C2/m$ transition is second order, or close to second-order in thermodynamic character (Salje, 1990). Additional strains, $+\varepsilon_2$, $+\varepsilon_3$ and $-\varepsilon_5$, all resulting in a volume strain, are associated with the M-site disordering at $T > 550$°C. The fact that both M-site ordering and the *P* to *C* transition induce measurable spontaneous strains provides a mechanism for interaction between each. We anticipate that changes in M-site order will induce changes in the characteristics of the $P2_1/m \rightarrow C2/m$ transition through the common strain interaction.

Acknowledgements

Dr P. Dunn of The Smithsonian Institute is thanked for kindly providing the cummingtonite sample. We would like to thank Dr Tiziana Boffa-Ballaran for her help and views throughout the writing of this paper. We gratefully acknowledge support from the NERC (grant number GR3/11741) and Rutherford Appleton Laboratory for providing beam time on ISIS.

References

Bown, M.G. (1966) A new amphibole polymorph in intergrowth with tremolite: Clino-anthophylite? *Amer. Mineral.*, **51**, 259–60.

Burns, R.G. and Strens, R.G.J. (1966) Infrared study of the hydroxyl bands in clinoamphiboles. *Science*, **153**, 890–2.

Ghose, S. (1961) The crystal structure of cummingtonite. *Acta Crystallogr.*, **14**, 622–7.

Ghose, S. and Ganguly, J. (1982) Mg-Fe order – disorder in ferromagnesian silicates. Pp. 1–99 in *Advances in Physical Geochemistry* **2**, (S.K. Saxena, editor). Springer-Verlag, New York.

Ghose, S. and Hellner, E. (1959) The crystal structure of Grunerite and observations on the Mg-Fe distribution. *J. Geol.*, **67**, 691–701.

Ghose, S. and Weidner, J.R. (1972) Mg^{2+}-Fe^{2+} order-disorder in cummingtonite, $(Mg,Fe)_7Si_8O_{22}(OH)_2$: A new geothermometer. *Earth Planet. Sci. Lett.*, **16**, 346–54.

Ghose, S. and Yang, H. (1989) Mn-Mg distribution in a C2/m manganoan cummingtonite: Crystal-chemistry considerations. *Amer. Mineral.*, **74**, 1091–6.

Hawthorne, F.C. (1983) The crystal chemistry of the amphiboles. *Canad. Mineral.*, **21**, 173–480.

Hawthorne, F.C. and Grundy, H.D. (1977) The crystal structure and site-chemistry of a zincian tirodite by least squares refinement of X-ray and Mössbauer data. *Canad. Mineral.*, **15**, 309–20.

Hawthorne, F.C., Della Ventura, G. and Robert, J.-L. (1996) Short-range order of (Na,K) and Al in tremolite: An infrared study. *Amer. Mineral.*, **81**, 782–4.

Henderson, C.M.B., Knight, K.S., Redfern, S.A.T. and Wood, B.J. (1996) Temperature dependence of octahedral cation site exchange in olivine determined by in situ, time-of-flight, neutron powder diffraction. *Science*, **271**, 1713–5.

Hirschmann, M., Evans, B.W. and Yang, H. (1994) Composition and temperature dependence of Fe-Mg ordering in cummingtonite-grunerite as determined by X-ray diffraction. *Amer. Mineral.*, **79**, 862–77.

Hull, S., Smith, R.I., David, W.I.F., Hannon, A.C., Mayers, J. and Cywinski, R. (1992) The POLARIS powder diffractometer at ISIS. *Physica B*, **180**, 1000–2.

Larson, A.C. and Von Dreele, R.B. (1994) *GSAS general structure analysis system.* LANSCE MS-H805, Los Alamos National Laboratory.

Leake, B.E., Wooley, A.R., Arps, C.E.S., Birch, W.D.,

Gilbert, M.C., Grice, J.D., Hawthotne, F.C., Kato, A., Kisch, H.J., Krivovichev, V.G., Linthout, K., Laird, J., Mandarino, J.A., Maresch, W.V., Nickel, E.H., Rock, N.M.S., Schumacher, J.C., Smith, D.C., Stephenson, N.C.N., Ungaretti, L., Whittaker, E.J.W. and Youzhi, G. (1997) Nomenclature of the amphiboles: Report of the Subcommittee on Amphiboles of the International Mineralogical Association, Commission on New Minerals and New Mineral Names. *Mineral. Mag.*, **61**, 295–321.

Maresch, W.V. and Czank, M. (1988) Crystal chemistry, growth kinetics and phase relationships of structurally disordered (Mn^{2+},Mg)-amphiboles. *Forts. Mineral.*, **66**, 69–121.

Mueller, R.F. (1970) Two-step mechanism for order-disorder kinetics in silicates. *Amer. Mineral.*, **55**, 1210–8.

Papike, J.J., Ross, M. and Clark, J.R. (1969) Crystal-chemical characterization of clinoamphiboles based on five new structure refinements. *Mineralogical Society of America Special Paper* **2**, 117–36.

Prewitt, C.T., Papike, J.J. and Ross, M. (1970) Cummingtonite: a reversible, nonquenchable transition from $P2_1/m$ to $C2/m$ symmetry. *Earth Planet. Sci. Lett.*, **8**, 448–50.

Redfern, S.A.T., Henderson, C.M.B., Wood, B.J., Harrison, R.J. and Knight, K.S. (1996) Determination of olivine cooling rates from metal cation ordering. *Nature*, **381**, 407–9.

Redfern, S.A.T., Harrison, R.J., O'Neill, H.St.C. and Wood, D.R.R. (1999) Thermodynamics and kinetics of cation ordering in $MgAl_2O_4$ spinel up to 1600°C from in-situ neutron diffraction. *Amer. Mineral.*, **84**, 299–310.

Rietveld, H.M. (1969) A profile refinement method for nuclear and magnetic structures. *J. Appl. Crystallogr.*, **2**, 65–71.

Ross, M., Papike, J.J., Shaw, K.W. and Weiblen, P.W. (1968) Exsolution in clinoamphiboles. *Science*, **159**, 1099–102.

Ross, M., Papike, J.J. and Shaw, K.W. (1969) Exsolution textures in amphiboles as indicators of subsolidus thermal histories. *Mineralogical Society of America, Special paper*, **2**, 275–99.

Salje, E.K.H. (1990) *Phase Transitions in Ferroelastic and Co-elastic Crystals*. Cambridge University Press, Cambridge.

Sears, V.F. (1992) Neutron scattering lengths and cross sections. *Neutron News*, **3**, 26–38.

Sokolova, E.J., Kabalov, Yu.K., McCammon, C., Schneider, J. and Konev, A.A. (2000) Cation partitioning in an unusual strontian potassicrichterite from Siberia: Rietveld structure refinement and Mössbauer spectroscopy. *Mineral. Mag.*, **64**, 19–23.

Sueno, S., Papike, J.J., Prewitt, C.T. and Brown, G.E. (1972) Crystal structure of high cummingtonite. *J. Geophys. Res.*, **77**, 5767–77.

Whittaker, E.J.W. (1949) The structure of Bolivian Crocidolite. *Acta Crystallogr.*, **2**, 312–7.

Yang, H. and Hirschmann, M.M. (1995) Crystal structure of $P2_1/m$ ferromagnesain amphibole and the role of cation ordering and composition in the $P2_1/m$–$C2/m$ transition in cummingtonite. *Amer. Mineral.*, **80**, 916–22.

Yang, H. and Smyth, J.R. (1996) Crystal structure of a $P2_1/m$ ferromagnesian cummingtonite at 140 K. *Amer. Mineral.*, **81**, 363–8.

[*Manuscript received 11 October 1999: revised 20 December 1999*]